Backscattering from a bio-aerosol measured with a coherent laser radar

FREDRIK KULLANDER

FOI, Swedish Defence Research Agency, is a mainly assignment-funded agency under the Ministry of Defence. The core activities are research, method and technology development, as well as studies conducted in the interests of Swedish defence and the safety and security of society. The organisation employs approximately 1000 personnel of whom about 800 are scientists. This makes FOI Sweden's largest research institute. FOI gives its customers access to leading-edge expertise in a large number of fields such as security policy studies, defence and security related analyses, the assessment of various types of threat, systems for control and management of crises, protection against and management of hazardous substances, IT security and the potential offered by new sensors.

FOI
Defence Research Agency
Sensor Systems
P.O. Box 1165
SE-581 11 Linköping

Phone: +46 13 37 80 00
Fax: +46 13 37 81 00

www.foi.se

FOI-R--2534--SE Scientific report
ISSN 1650-1942 July 2008

Sensor Systems

Fredrik Kullander

Backscattering from a bio-aerosol measured with a coherent laser radar

Titel	Bakåtspridning från en bioaerosol uppmätt med en koherent laserradar
Title	Backscattering from a bio-aerosol measured with a coherent laser radar

Rapportnr/Report no	FOI-R--2534--SE
Rapporttyp Report Type	Vetenskaplig rapport Scientific report
Sidor/Pages	36 p
Månad/Month	July
Utgivningsår/Year	2008
ISSN	ISSN 1650-1942
Kund/Customer	FMV
Forskningsområde Programme area	4. Sensorer och signaturanpassning 4. Sensors and Low Observables
Delområde Subcategory	42 Sensorer 42 Above surface Surveillance, Target acquisition and Reconnaissance
Projektnr/Project no	E 3381
Godkänd av/Approved by	Lars Bohman

FOI, Totalförsvarets Forskningsinstitut	FOI , Swedish Defence Research Agency
Avdelningen för Sensorsystem	Sensor Systems
Box 1165	P.O. Box 1165
581 11 Linköping	SE-581 11 Linköping

Sammanfattning

En kontinuerlig koherent laser radar med 2 W uteffekt vid 1.5 μm har använts för att mäta tillbakaspridningen från en bioaerosol. Aerosolpartiklarna som användes genererades från Turex, som är ett orenat tekniskt preparat med sporer av *Bacillus thuringensis* (BT). En serie laboratoriemätningar har genomförts. Mätavståndet var 28 meter. Aerosolen genererades i en duschkabin. Inne i duschkabinen hade ett rörsystem arrangerats för att cirkulera luften med partiklarna. En partikelräknare som räknade partiklar i storleksintervallet 0,5 to 10 μm anslöts till duschkabinen. En detekterbar bakåtspridningssignal kunde uppmätas för totala partikelkoncentrationer ned till 4000 partiklar per liter (ppl). Olika mått på styrkan i bakåtspridningssignalen togs fram. Ett medelvärde för bakåtspridningseffektiviteten, med antagande om att den är oberoende av partikelstorlek, bestämdes till $Q_\pi \approx 1$ med en relativt stor osäkerhet som uppskattades till en faktor 4. Resultatet motsvarar en detektionströskel på cirka 2000 ppl för partiklar med en typisk storlek på 2 μm. Det konstaterades att detektionströskeln för mätning med koherent laserradar är beroende av partiklarnas hastighetsdistribution vilket är en potentiell nackdel med tekniken. Detektionströskeln kan däremot i princip visas vara oberoende av såväl avstånd som mottagaraperturens storlek så länge partiklarna är jämt fördelade i mätvolymen. På längre avstånd kan dock fokusering med större optik än de 30 mm som användes här krävas för att begränsa mätvolymens längd till målets djup.

Nyckelord: koherent laser radar, lidar, avståndsdetektion, biologiska stridsmedel, bioaerosol, bakåtspridningskoefficient

Summary

A continuous wave coherent laser radar with an output power of 2 W at 1.5 μm was used to measure the backscattering from a bio-aerosol. The aerosol particles used in this experiment were generated from Turex, a non-pure technical preparation of spores of *Bacillus thuringensis* (BT). A series of measurements in a laboratory environment were performed. The distance to the aerosol was 28 m. The aerosol was maintained in a shower cabin incorporating a tube arrangement to circulate an air stream with the particles. A particle counter was connected to the cabin and particles in the size range from 0.5 to 10 μm were counted. A detectable backscattering signal was found for a total particle concentration ranging down to 4000 particles per liter (ppl). The backscatter signal was quantified in different ways. An average value of the backscattering efficiency for the particles, assuming it to be independent of size, was estimated to be $Q_\pi \approx 1$ with an uncertainty of a factor of four. The corresponding detection threshold for particles with a typical size of 2 μm is about 2000 ppl. It was realized that the detection threshold will be a function of the particle radial velocity distribution which is a potential drawback of the coherent laser radar for this application in practice. On the contrary, the detection threshold can in principle be shown to be independent of range and aperture size as long as the particles are uniformly distributed within the measuring volume. However gauging at longer ranges might require a larger optical aperture than the 30 mm diameter used in these tests in order to confine the focal length to the target cloud.

Keywords: coherent laser radar, lidar, stand-off detection, biological warfare agent detection, bio-aerosol, back-scattering efficiency

Contents

1. Introduction

This study followed our previous experimental work [1]. A bistatic continuous wave (CW) coherent laser radar (CLR) was used to detect the presence of aerosol particles of biological origin at a short range in a laboratory environment. In contrast to the previous work we now had access to a particle counter allowing comparison between the detected optical power and the number of particles within the scattering region. Like previously, a modified shower cabin was used to enclose particles in a target area but now a particle generator was incorporated in the setup.

2. Experimental work

Material and methods

A bistatic CLR system, outlined in figure 1, was used in these experiments. This system has been developed at FOI for remote vibration analysis [2]. The laser (Photonetics Nanotunics)

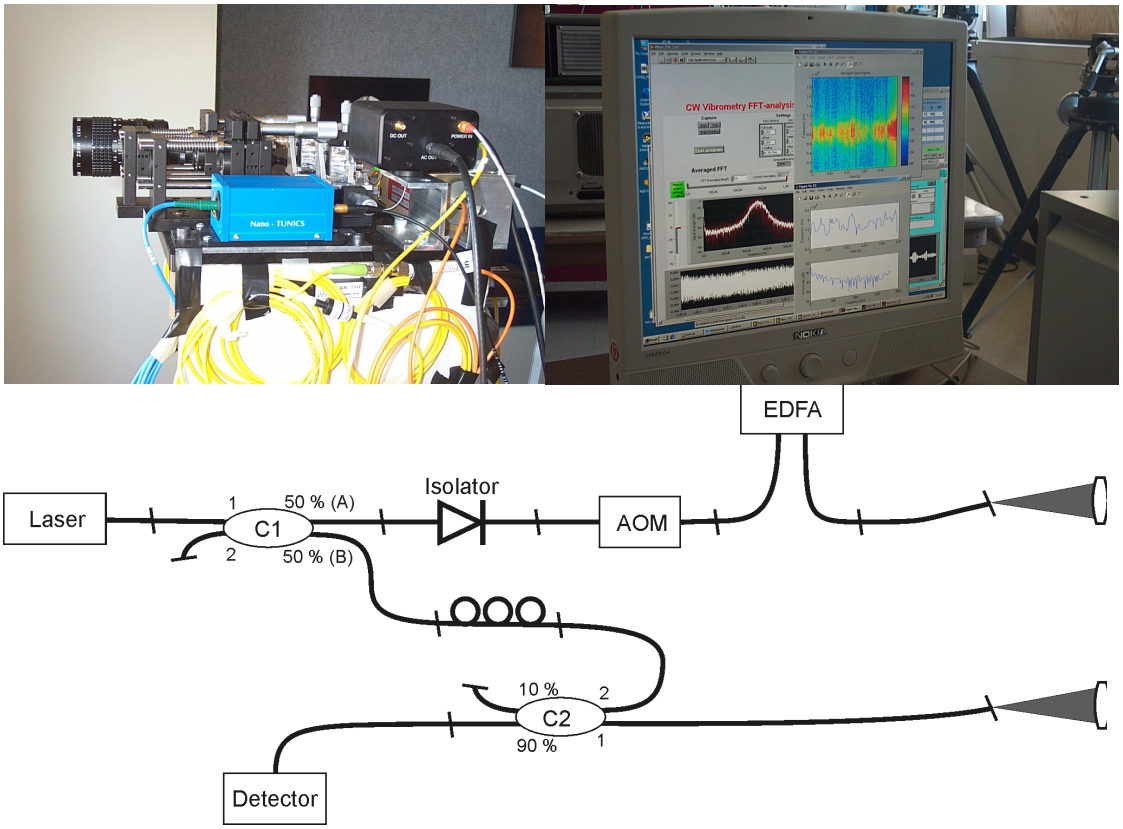

Figure 1. *Schematic drawing of optical part of laser vibrometer. The slashed lines stand for angled (FC-APC) connectors, C1 and C2 fiber couplers, AOM acousto optic modulator, EDFA erbium doped fiber amplifier.*

has an output power of 6 dBm (4 mW) at a nominal drive current of 75 mA and a wavelength of 1550 nm. The CLR system is constructed with the use of fiber optic components. The laser output beam is split in two parts in a 2x2 directional coupler (C1) of which a reference beam is passed through a polarization controller and further to a second directional coupler with a splitting ratio of 10:90 (C2). The second coupler directs about 10% of the reference beam to the output connected to the detector while 90% of the light incident on its other port is coupled to the same output. The reference field is mixed with the field from the receiving telescope in this coupler and the resulting intensity is monitored by a photo receiver (New Focus 1811-DC) with a conversion gain of 38 kV/W (measured over 50 Ω). The signals were recorded using a data acquisition PCI card (8 bit, 1 GSamples/sec, Acqiris PC-110) with an internal memory of 2 MSamples mounted inside a PC.

The outgoing signal beam pass through an isolator, (OZ Optics, FOPI-11-11-1550-9/125-S-60-3A3A-3-1-55) with an isolation of > 60 dB, to protect the laser source from backscattered light. An acousto-optic modulator (Brimrose, AMF-25-1550-2FP) is used to obtain a heterodyne signal at the receiver. It upshifts the optical frequency of the output beam by +25 MHz. An Erbium doped fiber amplifier (IPG Laser GmbH, EAR-2-C) is finally used to amplify the beam to an adjustable output power level up to 2 W. The transmitting and the receiving ports are identically arranged. A lens, 30 mm in diameter, with a focal length of f = 101 mm is positioned at a distance from an APC fiber connector close to the focal length to provide a collimated output beam at the output port and a focus on the fiber tip at the input port. The transverse position of the input port is adjustable, making it possible to change the crossover location of the output beam and the input acceptance cone. The nominal distance between the two ports is 50 mm. The optical head as shown in figure 1 is mounted on a tripod and can be rotated and tilted with PC-controlled stepper motors from Physik Instrumente. A CCD-camera for pointing is coaligned with the telescopes.

The measurements were performed in our laboratory according to figure 2. The work was carried out during three days of which the first was used mainly to set up the equipment and make a few initial measurements. The shower cabin previously used was now modified to work as a chamber enclosing bacteriological particles. The cabin was laid down 28 meters from the CLR. It was carefully sealed apart from two holes with a diameter of about 2 cm, at the front and the

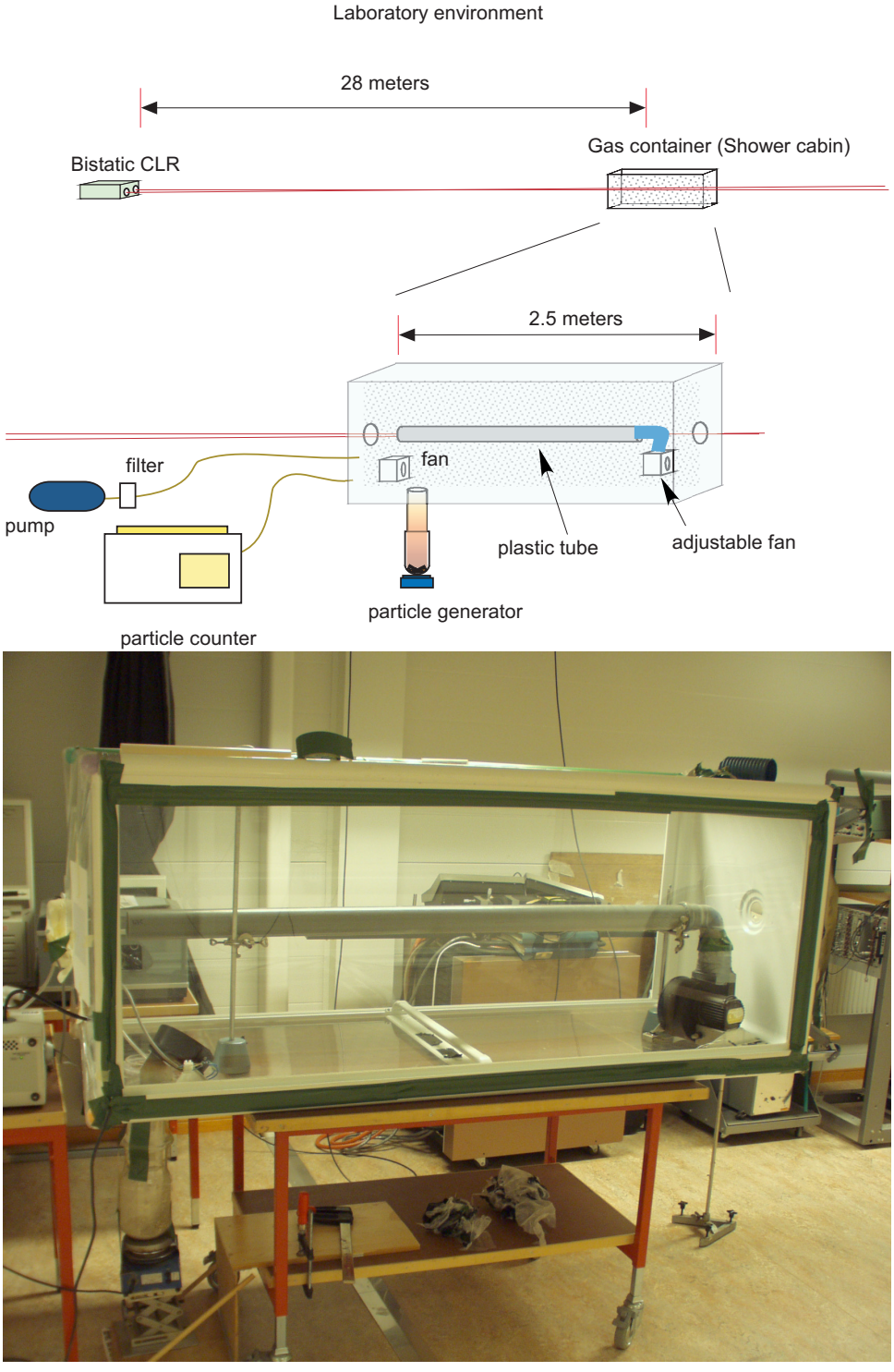

Figure 2. *Experimental arrangement for the detection of bacteriological test particles.*

rear of the cabin, in the laser line of sight. The principle scattering volume constituting the active region of the CLR is depicted in figure 3. The output laser beam and the field of view of the receiving telescope were adjusted to cross at the measuring distance. A scattering volume

with the shape approximately of a double cone is formed. Laser light scattered in this volume contribute effectively to the received optical power.

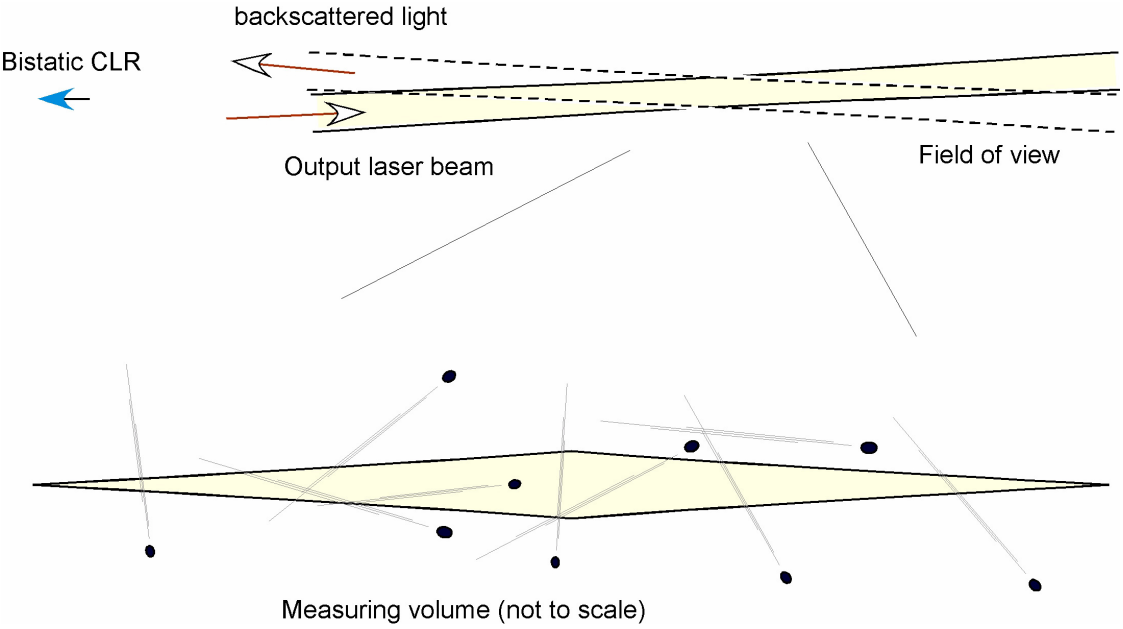

Figure 3. *The bistatic CLR has a measuring volume defined by the intersection between the output laser beam and the field of view of the receiving telescope.*

The particles used in these experiments came from Turex, a non-pure technical preparation of spores of *Bacillus thuringensis* (BT) [3]. These are class 1 organisms often used as simulants for BWA. The particles consist of clusters of the spores contaminated with various impurities [4]. No microscopic examinations were done at this time. A photo depicting a washed organism, *Bacillus atrophaeus* (BG), of a similar kind from a previous examination is shown in figure 4.

The particles were continuously fed to the shower cabin by a generator arrangement connected to the cabin. The generator was simply a glass bowl containing the bacteriological powder in the bottom. The powder was raised to the air by means of a magnetic stirrer with an adjustable speed in the bottom of the bowl. A primary fan in the cabin was used to circulate the raised particles. The speed of the stirrer regulated the particle concentration in the cabin. A pump connected to the cabin through a filter was used to keep the cabin pressure slightly lower than the ambient pressure. Therefore particles were continuously lost through the pump in addition to those anticipated to be lost by sticking to the surfaces in the shower cabin. A particle counter was also connected to the cabin to monitor the particle concentration. One counting event was

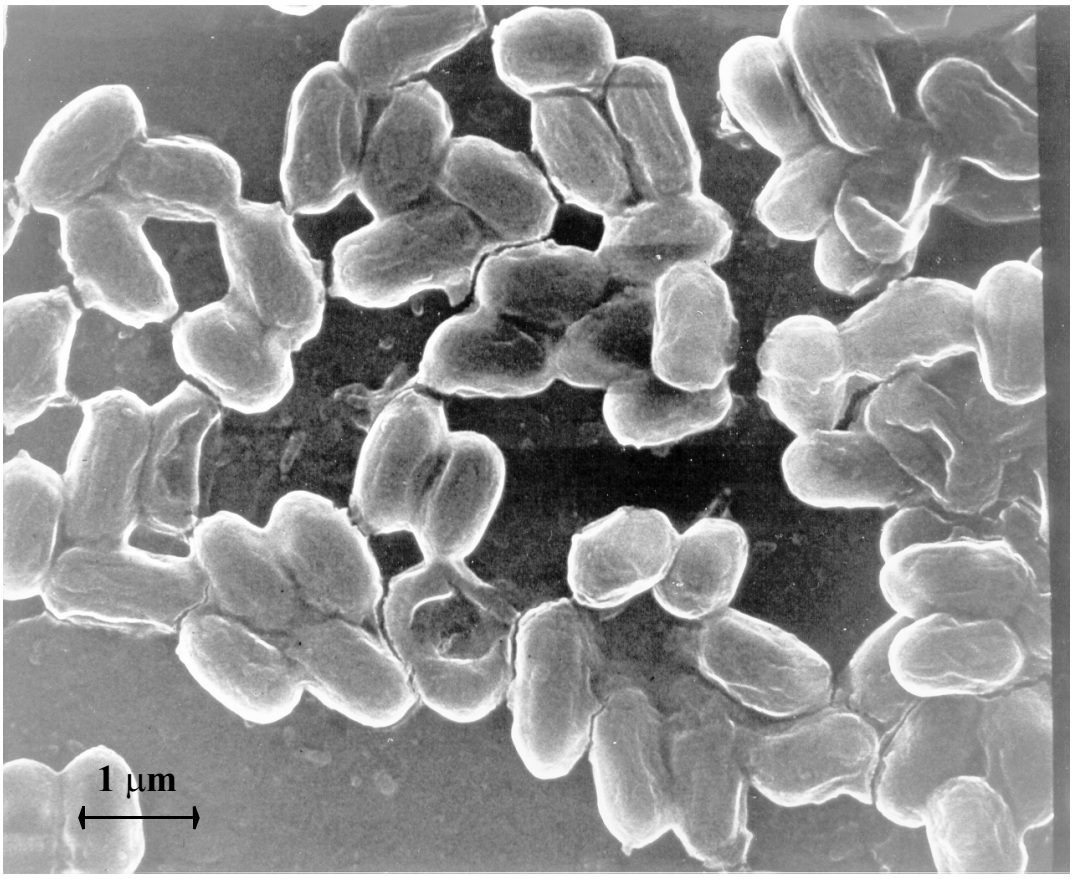

Figure 4. *Clusters of Bacillus atrophaeus, BG. The bean like objects are the spores measuring approximately 1 μm in length.*

averaged over 20 seconds. Particle concentration values for sizes around 0.5, 1, 2, 3, 5, 10 μm were registered.

Initially, a practical problem was that stationary particles were not introducing an optical doppler shift. The unshifted heterodyne signal coincided with a residual peak, due to electrical crosstalk, around the nominal carrier frequency at 25 MHz. Hence, after some initial tests a plastic tube, 70 mm in diameter, was placed in the cabin in order to circulate the air in the cabin so that most particles generate a Doppler shifted signal. The plastic tube was centred along the laser line of sight with the inlet side facing the CLR. The rear side was connected to the fan by a 90 degree bend, see figure 2. The inlet of a second, adjustable, fan was connected by its inlet side to the tube. A hole was opened up in the tube wall of the bend in the line of sight of the CLR.

An optical output power of 2 W was used from the middle of the second day after which the

data being analysed were taken. The focus and the intersection of the output beam and the receiver field of view were adjusted manually. We covered the rear shower cabin hole with scotch to obtain a relatively strong signal upon which it was possible to optimize the adjustments of the CLR. Additionally, the aim point and the focus of the transmitting and the receiving telescopes were compared by connecting light out through both telescopes. A fluorescent plate was used to monitor the infrared light spots.

The experiments were performed mainly with the CLR focused in the cabin. The signal power dropped significantly when the focus was changed.

Results

Particle generation

For reference, the particle concentrations were measured in the laboratory environment and in the closed shower cabin before generating particles. The typical concentration levels during the measurements are compared to these background values in table 1. Note that it was possible to reduce the concentration in the cabin well below the ambient level. The particle concentration in the laboratory decrease as a function of particle size and we can see that the concentration levels in the closed shower cabin, after a night without particle production is about a factor of ten below the laboratory concentration. The typical concentration level during particle production was much higher than the laboratory concentration for the larger sized particles but not for the smallest, 0.5 μm, particles. A full set of particle counter data can be found in table 2, page 24.

Table 1. Particle concentration levels in units of particle per liter (ppl)during the measurements.

size in μm	0.5	1	2	3	5	10	
laboratory	2000	600	120	30	10	2	ppl
shower cabin, no particles	120	40	15	6	1	0	ppl
typ. concentration level day 2	800	1300	3000	4000	4000	400	ppl
typ. concentration level day 3	1500	3300	4500	7000	8500	1700	ppl

Particles larger than 10 μm were not counted. Therefore, it was desired to assure that only a negligible amount of larger particles were generated. It was indeed possible to adjust the particle generator so that it raised predominantly smaller particles. The number of raised particles was expected to be a function of size with a steep knee at a certain particle size depending on

the adjustments of the generator [4]. We tried to keep the number of 10 μm particles less than a fraction of 1/10 of the number of the 5 μm particles. However, as evident from table 1, during the third day this was compromised in order to reach a higher overall concentration level. In neither case it can be guaranteed that the fraction of larger particles in the cabin was negligible with respect to the backscattered optical power and it remains a source of uncertainty.

Acquired waveforms

The waveforms consists of 500000 data points acquired at a sample rate of 100 Msamples/s, thus representing a 5 ms time window. The power spectral density (PSD) of acquired waveforms, shown in figure 5, explain the general features of the CLR return signal. The spectra were calculated using the Matlab function ”*pwelch*” which provides an estimate of the PSD using Welch’s method of averaged periodograms [5]. A window equal to the discrete Fourier transform (DFT) length of 16384 data points was used over the full length of the waveforms to obtain the averaged PSD estimate.

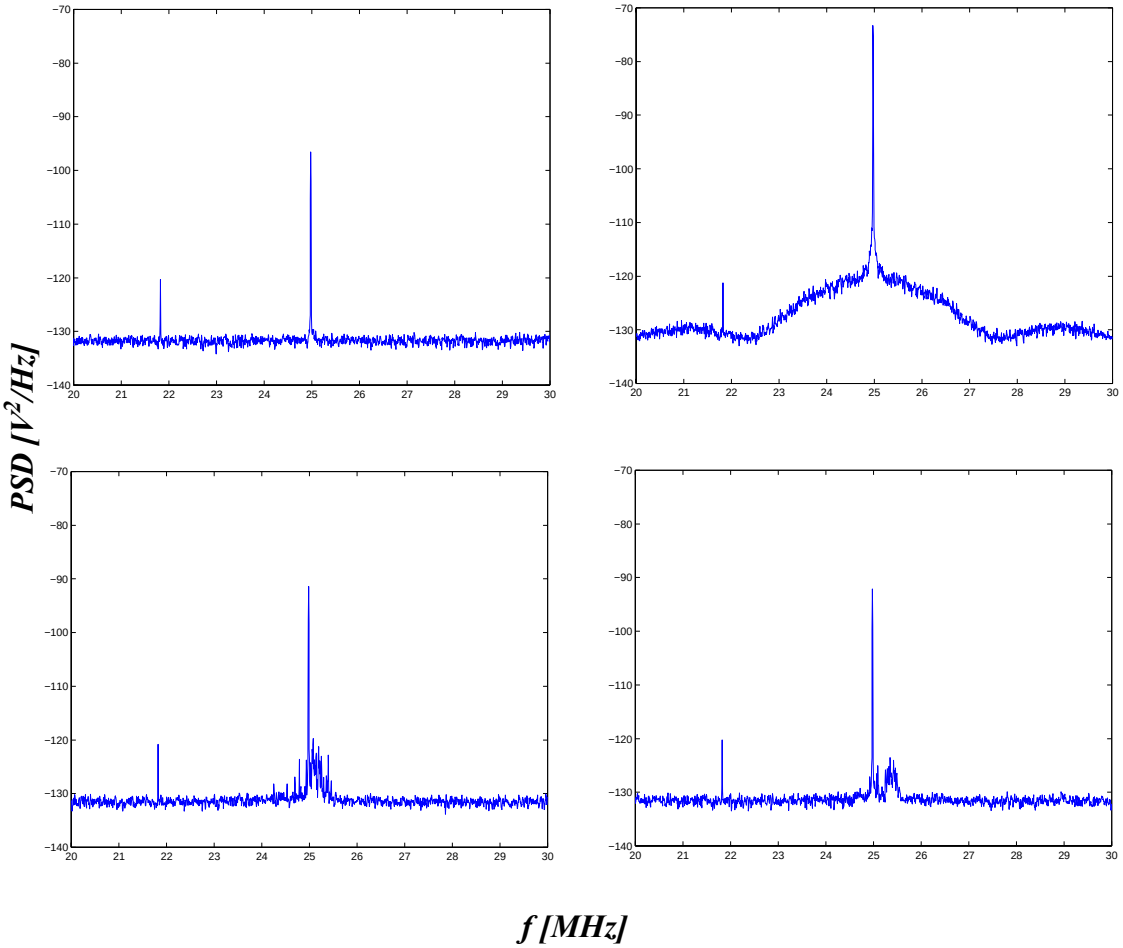

Figure 5. *Power spectral density of acquired waveforms. Top left; No particles (020312,1155). Top right; Tape covering the rear cabin hole (020312,1158). Bottom diagrams; Particles generated (020312,1158).*

In the absence of externally reflected light essentially a flat noise spectrum due to shot noise is expected. The upper left diagram shows the power spectral density of such data. Two peaks remain in the frequency band around the carrier frequency of 25 MHz. The peak at the carrier frequency itself is due to electrical crosstalk, possibly due to RF pick-up radiating from the acousto-optic modulator driver. The second peak at about 22 MHz has unknown origin and can be regarded as a temporal disturbance (it disappears in later measurements). The flat noise level at about -132 dB V^2/Hz is in good agreement with the expected shot noise level when taking into account the optical power level at the detector, measured to be 0.1 mW.

The upper right diagram shows the power spectral density of the signal received with a piece of scotch tape used as a target in the CLR focal volume at about 28 meters. In this case the optical signal generates a broad spectrum centred around the carrier frequency in addition to the nar-

row spike. The level and form of the broad signal part depend on the range to the backscattering target and arise due to phase jitter originating in the laser frequency noise. As expected the shape of the phase noise spectrum follows a $sinc^2(f)$ function centred around the carrier frequency.

The lower diagrams show the PSD of initial acquisitions with backscattered light from particles in the cabin. The signal power is distributed around the carrier frequency. In this case we see the power distribute a few hundred kHz around the centre frequency corresponding to a velocity distribution ranging from approximately -0.1 m/s to 0.1 m/s. The detected backscattered power in this example was comparably low since the data was acquired before optimizing the CLR settings. Expectably, the measured signal power turned out to be critically dependent on the focusing and the alignment of the CLR. To optimize the measuring volume two steps were used. Firstly, the longitudinal postion of both the transmitter and the receiver focus were adjusted to the centre of the shower cabin. Secondly, the overlap in the intersection region was maximized by tuning the receiving port aspect angle based upon the measured heterodyne signal level.

The SNR of the waveforms recorded after these adjustments was much better than before, see figure 6. The spectra show measurements during the second day when the fan was running to circulate the particles. Apart from the spike at 25 MHz a broader range of signal power is distributed around 24 MHz. This indicates that the particles are moving with a velocity of about 0.7 m/s (1.29 MHz/m/s) away from the CLR These examples bring out two general cases that

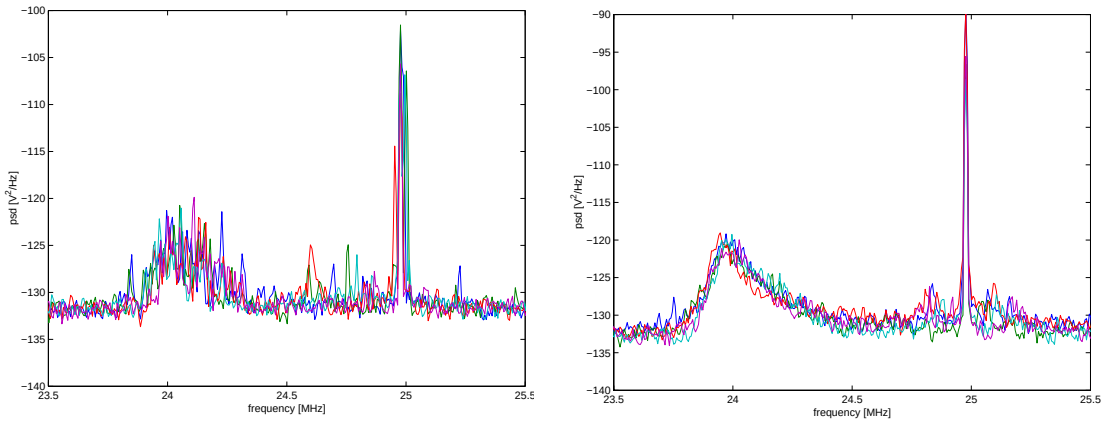

Figure 6. *Power spectral density of heterodyne signals registered with the CLR focused in the cabin. The circulation fan was running at low speed. Observe that the diagrams contain overlaid spectra of 5 consecutive waveforms. The data were taken during the second day at about 14.30.*

appeared. The heterodyne signal distributes in the frequency domain either as distinguishable spikes like in the left hand diagram or as a continuum around a centre frequency such as in the right hand diagram. A possible reason for these variations might be that the particles move in different ways depending on the flow dynamics in the cabin.

The signal level rapidly decreased when the CLR was defocused. The spectra in figure 7 were acquired with the CLR telescopes defocused so that the spot size at the rear of the cabin was approximately 20 mm in diameter. The signal power originating in moving cabin particle is hardly detectable at this spectral resolution. The remaining measurements were performed with the CLR focused.

The following diagrams summarize the appearance of the waveforms at the remaining measurements. Data acquired with the circulation fan running at different speeds are shown in figure 8. The heterodyne signal spectrum is distributed mainly around a frequency offset, from 20 to 24 MHz, associated with the particles moving with the air flow in the tube. In addition spectral power distribute around, or even slightly above, 25 MHz which might be associated with particles in the line of sight of the laser beam but outside of the circulation tube. Judging from the spectral data these particles move predominantly towards the CLR in some region of the shower cabin, possibly in the shower cabin front side hole.

Data at different concentration levels where acquired while the circulation fan was running at constant speed. The particle generator was simply turned off after which a series of acquisitions were made. We see in figure 9 how the signal power evolves during 15 minutes after shut down.

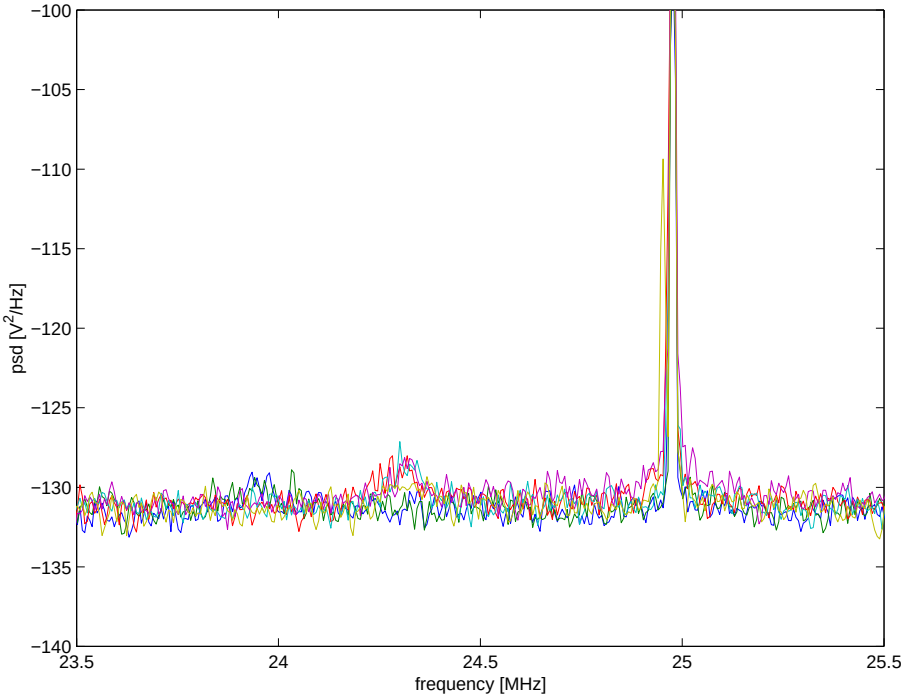

Figure 7. *Power spectral density of optical signals registered with the CLR defocused. The circulation fan was running at low speed. The data were taken during the second day at about 15.00.*

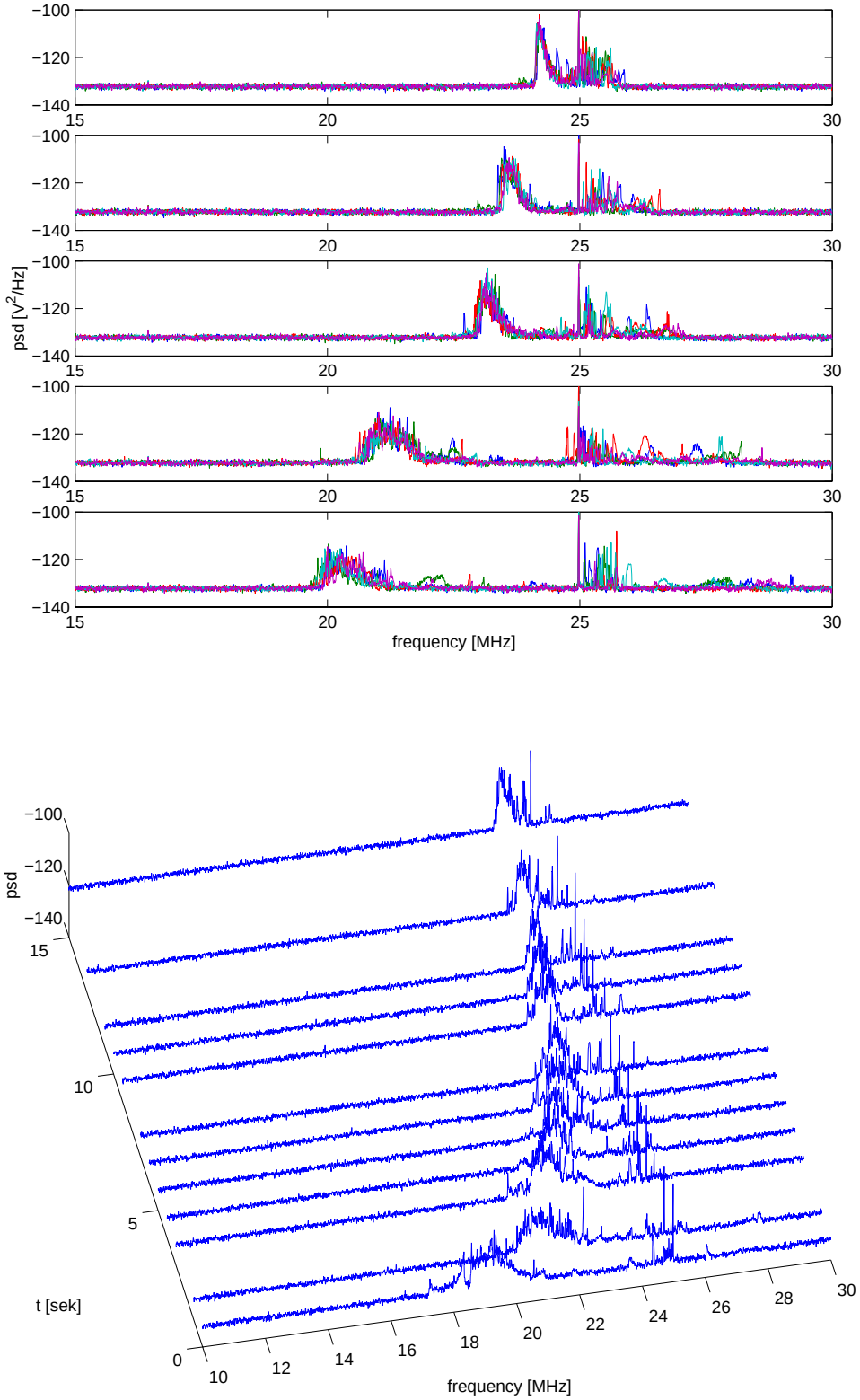

Figure 8. *Power spectral density at different particle velocity distributions. The upper diagrams shows waveforms taken at different fan speeds. The lower diagram shows the PSD evolution after turning off the fan. The data were acquired the third day at 10.00.*

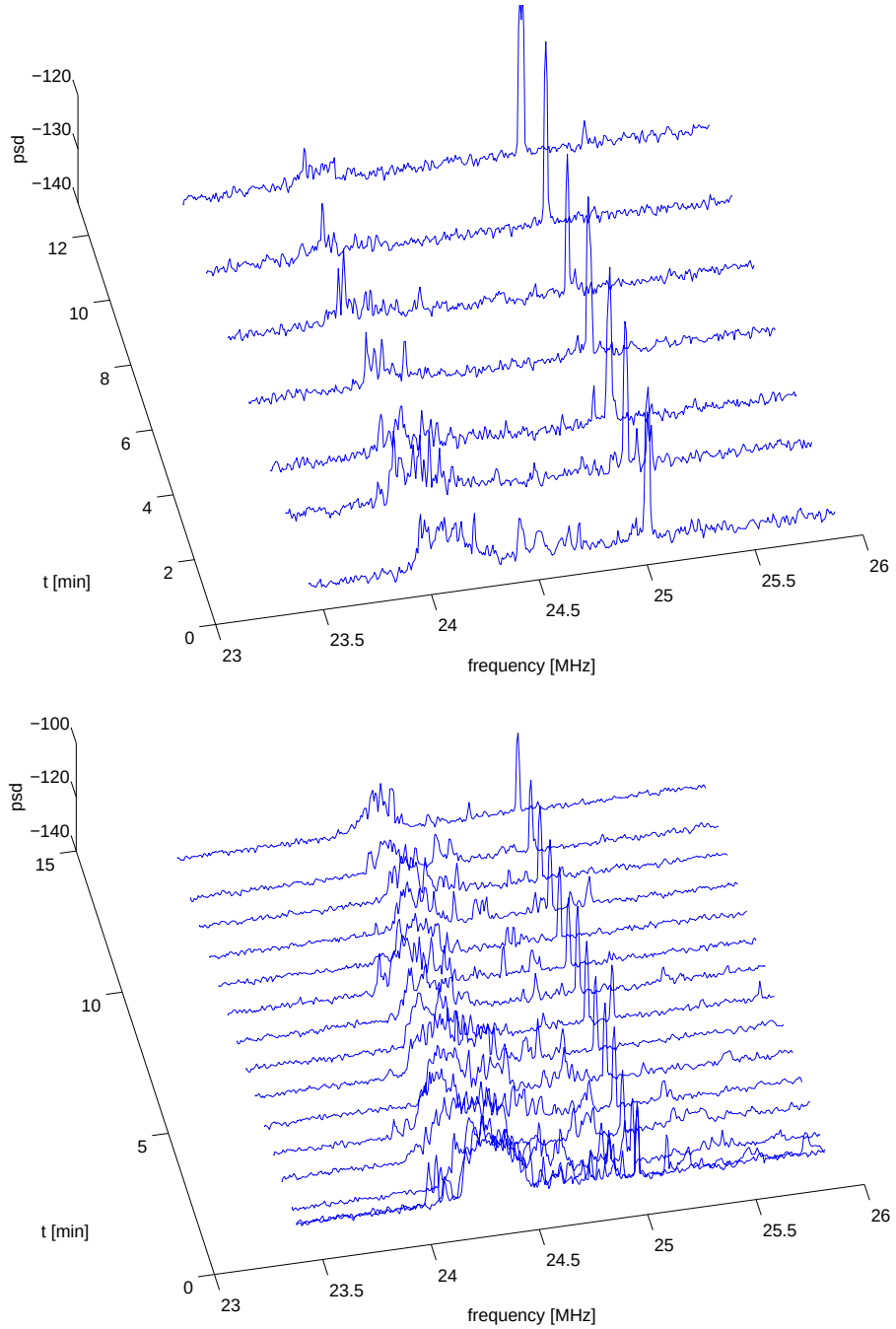

Figure 9. *Time evolution of power spectral density after turning off the particle generator. The upper diagram shows data from day 2 around 10.30 (when the maximum particle concentration was lower). The lower diagram shows data from day 3 around 12.00.*

An estimate of the received optical power was obtained by integration of the spectral power that was exceeding a predetermined threshold excluding the signal power at 25 MHz, see figure 10. Since the CLR noise level was stable and flat in the frequency region of interest a constant integration threshold could be applied at $8*10^{-14}$ V^2/Hz (-131 dB V^2/Hz), close to the level of the shot noise.

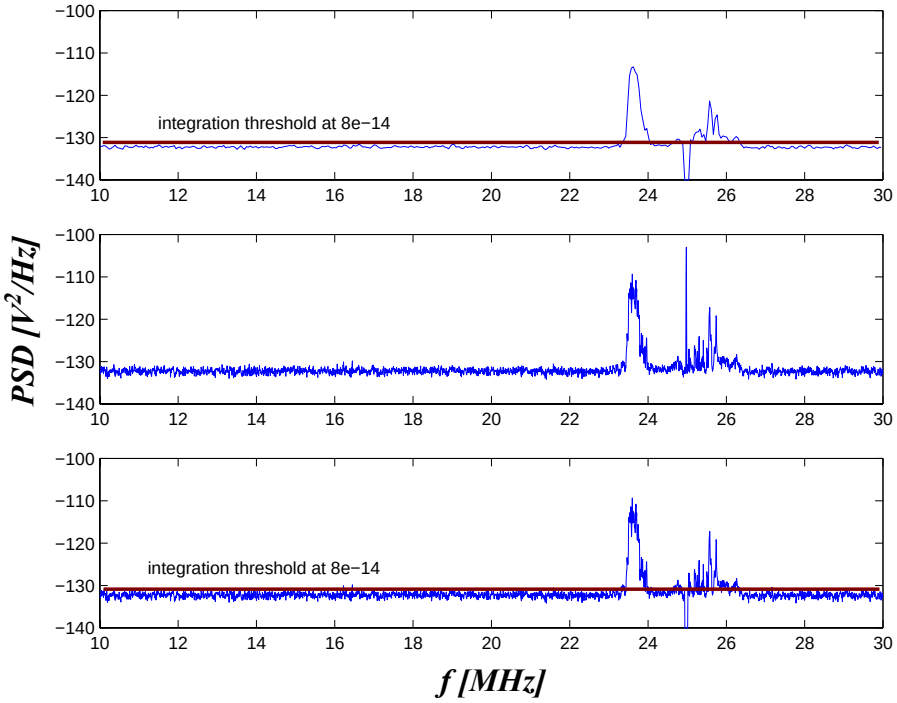

Figure 10. *Integration of spectral power. The middle diagram shows the unmodified PSD using a window of 16384 samples. The integrated power is calculated at two spectral resolutions. The top (2046 samples) and bottom (16384 samples) diagrams display the modified data set with the power at 25 MHz removed.*

The integrated power (in the frequency domain), in a band from 10 to 30 MHz was used as a measure of the total heterodyne signal power originating from backscattering in the measuring volume. The integration was made at two spectral resolutions. The higher resolution bandwidth (RBW) of 12 kHz was obtained with the previously used settings for the window and DFT length, i.e. 16384 samples. A lower RBW of 100 kHz was obtained by reducing both lengths to 2048 samples. It was found that the estimated heterodyne signal power was dependent on the choice of resolution. In particular at low power levels approaching the noise.

In figure 11 the signal power calculated as above is compared to the particle counts registered throughout th tests. Since the particle counter data and the CLR data were acquired independ-

ently there are not always data points simultaneously.

During the second day, between 12 am and 5 pm (2100 and 2400 in the local time scale of the diagrams), the particle concentration was generally lower than during the third day. We observe that the estimated heterodyne signal power obtained at low spectral resolution is lower than the higher resolution values throughout the data of this day. A similar difference appears during the third day at low particle concentration counts. Hence, it seems natural to associate the ambiguous power estimate with a low signal level.

The two first particle counter data sets show the particle concentration in the cabin before turning on the generator. The concentration is much lower than the laboratory concentration after a night without running fans. After starting the particle generator all counts immediately rise. With reference to the time scale of the diagram, the flow tube was mounted at 2200 minutes (13:48 day 2). The laser output power was 1 W until 2300 minutes when it was increased to 2 W. During 12 minutes from 2310 to 2322 a first acquisition session after turning off the particle generator was carried out. The concentration of 10 micron particles decreased by a factor of ten, the 5 micron particles by almost a factor of four and the smaller particles by about a factor of two. The RBW=100 kHz estimate of the heterodyne signal power decreases by a factor four while the RBW=12 kHz estimate decreases less than a factor of two. The last data during the second day were acquired before and after restarting the particle generator and when the laser beam was defocused. The particle generator was modified to generate more particles during the third day. We see that it was possible to achieve a concentration of more than 1000 particles/litre in all size fractions. It was feasible to further enhance the particle generation but not without increasing the relative fraction of the large particles. The generator was adjusted to produce a relative concentration of the 10 micron particles not exceeding a quarter of the 5 micron particles.

The first laser data during this day (around 3370 minutes) were captured with a defocused laser beam. From 3400 to 3420 minutes the CLR focus was optimized. Data at different flow velocities were acquired around 3440 minutes. The estimated heterodyne power did not change much with flow velocity. At about 3445 minutes the particle generator was turned off after which data where acquired during 20 minutes. The generator was turned on again after about an hour and then turned off again followed by a last series of acquisitions. We see in these trials that the heterodyne signal power drops significantly with time. We note that the drop exceeds

that of the concentration of smaller particles and resembles that of the 10 micron particles, in particular when measured at the 100 kHz resolution. The 12 kHz data falls somewhere in between.

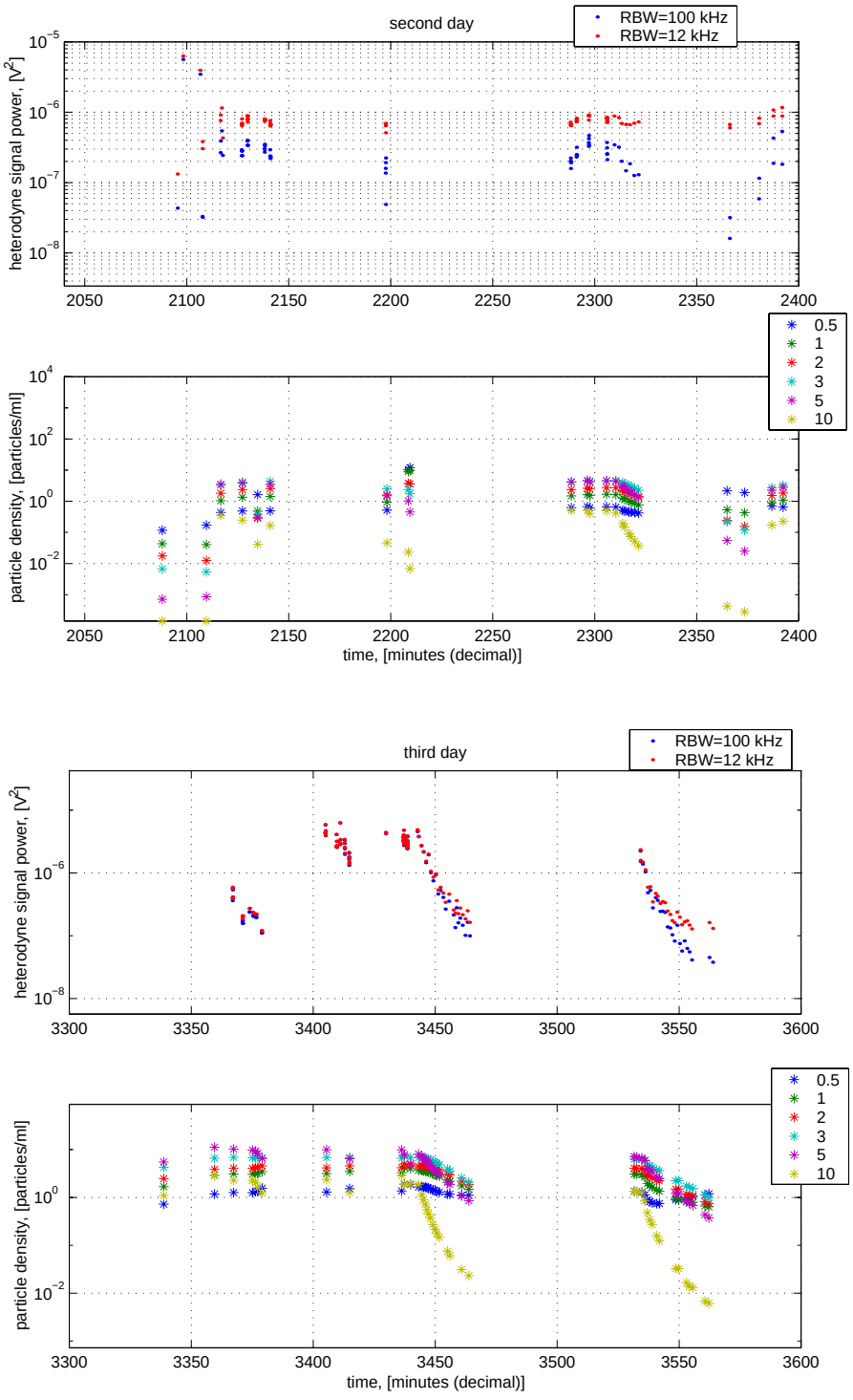

Figure 11. *Overview of acquired data. The time scale is given in minutes starting from one o'clock the first day. Thus, 2100 and 3540 minutes correspond to noon the second and the third day respectively.*

Table 2. Acquired particle concentrations given in the unit particles/liters (ppl).

Date	time	0.5	1	2	3	5	10	m	ppl tot	Comments
2002-03-11	16:09:54	924	659	885	1439	906	25		4812	In the showercabin
	16:08:48	2274	636	127	29	11	2		3077	In the laboratory
	16:35:36	687	1618	2569	4597	5147	444		14619	After particle generation, at shutdown
	16:40:20	642	1332	2182	3918	4122	296		12195	After particle generation, after shutdown
2002-03-12	11:48:02	117	43	18	7	1	0		185	Before particle generation, in the cabin
	12:09:40	170	40	12	5	1	0		229	
	12:16:43	437	1044	1810	3264	3502	354		10057	After particle generation, in the cabin
	12:27:16	488	1338	2366	4131	3817	247		12141	
	12:40:55	495	1431	2530	4326	3518	167		12299	
	13:48:38	10359	8981	3717	2403	1022	23		26481	After mounting flow tube in the cabin
	13:49:25	11933	9735	3582	1742	452	7		27443	
	15:08:33	624	1479	2358	4034	4215	515		12710	Changed flow direction in the tube
	15:16:22	669	1628	2618	4542	4644	514		14101	
	15:17:34	616	1541	2550	4429	4185	408		13321	
	15:25:46	668	1673	2746	4579	4537	493		14202	Output power increased to 2 W
	15:30:21	650	1624	2723	4599	4360	420		13956	After turning off the particle generator
	15:33:42	515	1260	2280	3971	3106	192		11132	
	15:34:39	486	1168	2117	3664	2816	149		10251	
	15:36:46	453	1033	1843	3211	2179	89		8720	
	15:37:42	445	971	1765	2985	1967	74		8133	
	15:39:36	437	839	1585	2614	1598	52		7073	
	15:41:31	420	753	1412	2242	1298	37		6125	
	16:24:53	2167	529	243	222	54	0		3216	Defocused laser beam. Before particle
	16:33:30	1901	426	156	118	25	0		2626	regeneration.
	16:46:49	699	898	1533	2697	2281	172		8107	Defocused laser beam. After particle
	16:52:20	651	1082	1831	3224	2773	228		9561	regeneration, in the cabin
2002-03-13	08:38:42	725	1674	2466	4249	5504	1096		14618	Defocused laser beam. Increased particle conc.
	08:59:32	1175	2891	3860	6627	11147	2858		25701	by modifying the generator.
	09:07:24	1261	3091	4094	6896	10186	2287		25528	
	09:15:07	1251	3064	4045	6743	9752	2275		24855	
	09:16:24	1328	3102	4173	6788	9321	2021		24711	Defocused laser beam. Increased particle conc.
	09:17:15	1333	3156	4244	6934	8359	1604		24026	by modifying the generator.
	09:19:03	1558	3482	4578	6727	6465	1239		22811	
	09:45:29	1292	3138	4151	6834	9948	2355		25364	Focusing laser beam again!
	09:54:57	1524	3505	4576	6768	6448	1265		22821	
	10:16:16	1364	3281	4171	6617	9851	2838		25284	Varying circulation fan speed
	10:17:22	1896	4192	5040	7347	7846	1834		26321	
	10:19:54	1862	3985	4780	6848	5059	1927		22534	
	10:23:13	1656	3674	4534	6794	8049	1845		24706	After turning off the particle generator
	10:24:31	1662	3669	4647	6785	7187	1155		23949	
	10:25:11	1635	3595	4564	6730	6648	903		23172	
	10:26:01	1649	3551	4538	6571	6008	723		22317	
	10:26:38	1599	3505	4501	6325	5532	551		21462	
	10:27:14	1560	3434	4423	6295	5104	446		20817	
	10:28:06	1502	3290	4294	6003	4666	368		19755	
	10:29:04	1433	3141	4151	5688	4115	269		18528	
	10:29:59	1396	3010	4011	5377	3694	216		17487	
	10:30:40	1316	2858	3839	5200	3365	177		16578	
	10:31:41	1290	2771	3665	4817	2988	146		15531	
	10:35:01	1173	2306	3080	3905	2080	76		12544	
	10:36:02	1164	2172	2937	3591	1845	60		11709	
	10:40:51	1115	1744	2180	2554	1081	31		8674	
	10:43:46	1115	1481	1874	2082	850	23		7401	
	11:51:38	1346	3062	4068	6340	7147	1347		21961	Turning on the particle generator
	11:52:33	1320	3065	4027	6295	6892	1310		21598	Before turning off the particle generator
	11:54:45	1291	2978	4038	6221	6638	1244		21166	After turning off the particle generator
	11:55:59	1136	2670	3748	5974	5924	846		19452	
	11:56:59	878	1958	2939	4642	4040	477		14458	
	11:57:56	820	1784	2768	4519	3750	344		13641	
	11:58:56	767	1641	2624	4312	3399	274		12744	
	12:00:50	743	1428	2327	3729	2727	158		10955	
	12:01:56	742	1352	2227	3623	2472	124		10416	
	12:08:36	897	966	1489	2232	1210	33		6794	
	12:09:52	885	945	1488	2257	1198	33		6773	
	12:13:04	997	809	1163	1731	838	17		5538	
	12:14:08	1023	817	1120	1629	762	14		5351	
	12:15:42	1043	791	1092	1549	679	13		5155	
	12:20:36	1133	663	821	1129	435	7		4181	
	12:22:14	1197	637	750	989	375	6		3949	

Finally, some of the data are presented in the time domain. The graphs in figure 12 show time sequences from the first of the particle generator shutdown trials during the third day. The displayed data have been digitally bandpass filtered from 23.8 to 24.8 MHz in order to distinguish signal features associated with the backscattered light from the residual peak at 25 MHz. The panner shows 1/5 of the full acquisition and the main diagrams is a zoom displaying 0.12 ms sequences. The data in the top diagram was acquired just about when the generator was turned off. The heterodyne signal periodicity of about 40 ns is much shorter than the resolution in the graphs leading to a dense pattern. However, the interesting characteristic in the time domain of the signal is in what way the carrier is modulated since it might tell something about the properties of the ensemble of scattering particles. The amplitude modulation ranges up to a peak voltage of about $4*10^{-3}$ V and come in bursts on a typical time scale of $1*10^{-5}$ s. The middle diagram shows data captured about 2 minutes later. The main difference is that the maximum modulation amplitude has decreased by a factor of 2 to about $2*10^{-3}$ V. Notable is also that the general burst time scale seems shorter which in part may be due to the noise which has a standard deviation of $2.5*10^{-4}$ V for these filtered signals. The comparison becomes similar for the two lower diagrams. The maximum modulation amplitude drops by another factor of 2 and the signal gets more noisy.

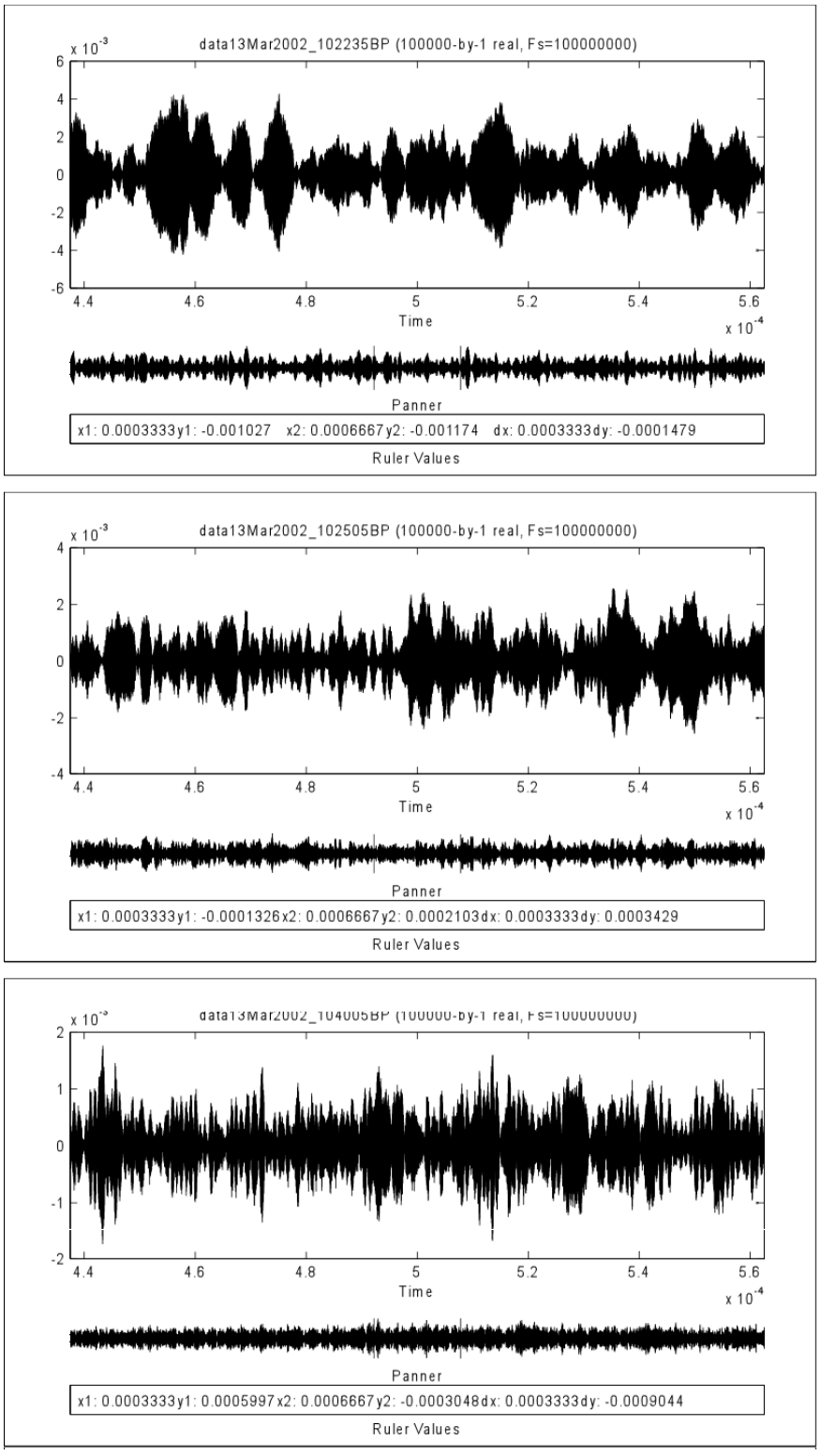

Figure 12. *Heterodyne signal power as a function of time for three acquisitions while the particle concentration was decreasing. Only a part of the full 5 ms acquisitions is shown. The diagrams range about 0.12 ms (the panner windows displays 1 ms of data).*

3. Discussion & analysis

The particles used in these tests were shown to be detectable at a range of 28 meters down to total particle concentration levels of approximately 4000 ppl. This particle concentration level was found simply by recognizing that significant heterodyne signal power was detected at this level. The detection threshold might be much lower, depending on the size distribution of the particles. Therefore a more generally applicable threshold cannot be established without further analysis.

To proceed with a more detailed analysis an average estimate of the volume backscatter function, β [$m^{-1}sr^{-1}$], can be obtained from the data. Acquisitions from the third day at about 10:17 (3437 minutes) are used for this estimate. These data files were acquired at different flow velocities with optimized CLR settings. The mean heterodyne optical power measured in the data was compared to the particle concentration counts taken at 10:16:16 and 10:17:22. These particle concentration counts were not taken at the same time as the CLR data so the mean value of the two data sets is used as an estimate of the actual particle concentration at 10:17.

The backscattered optical power can be approximated by the relation

$$P_r = I\Omega\beta V, \tag{3}$$

where I [W/m^2] is the intensity of the light impinging on the scattering volume, V [m^3], and where Ω [sr] denotes the solid angle defining the light cone collected by the receiving telescope. Hence, since we are able to estimate the system parameters I, V and Ω for this particular setup we can calculate β. Like previously [1] we relate the heterodyne signal power to the backscattered optical power by

$$U_{rms}{}^2 = \gamma^2 G^2 P_{lo} P_r, \tag{4}$$

where γ is the fringe visibility factor accounting for polarisation fading. We assume $\gamma \approx 0,7$. G is the conversion gain for the receiver and P_{lo} = 0.1 mW is the measured local oscillator optical power. Thus the volume backscatter function is related to the measured heterodyne signal power by

$$\beta = \frac{U_{rms}^{\ 2}}{\gamma^2 G^2 P_{lo} I \Omega V} \tag{5}$$

The average heterodyne signal power during the measurements under consideration was $3\pm1*10^{-6}$ V^2 resulting in $\beta \approx 3.9*10^{-5}$ $m^{-1}sr^{-1}$ with an uncertainty of about 30% being due to the variance in the measured values of the heterodyne signal power. The intensity was calculated as $I = P_{out}/\pi w_0^{\ 2}$, the solid angle as $\Omega = \pi D^2/4R^2$ where D is the effective telescope diameter and R the range, the scattering volume as $V = 4\pi w_0^{\ 3} R/3d$ where d is centre to centre distance between the transmitting and receiving lens, see figure 13. The beam waist radius, w_0, was found by using the relation, $w_0 = 2R\lambda/\pi D$, which applies for Gaussian beams [6]. Finally, $D = 2fNA$ where $f = 101$ mm is the focal length of the output lens and $NA = 0.13$ is the fiber numerical aperture.

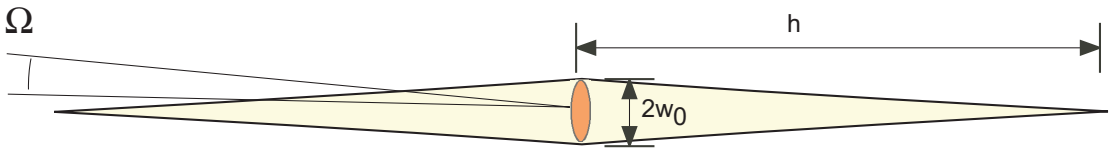

Figure 13. *Dimensions of measuring volume, V. Approximately a double cone with base radius, w0, and height, h. With our current parameters; V=2.7 cm^3.*

An average backscatter cross section, $\sigma_{\pi,avg}$, can be designated to the particles by dividing the volume backscatter function by the total particle concentration (for all sizes)

$$\sigma_{\pi,avg} = 4\pi\frac{\beta}{N_{tot}} \ [m^2]. \tag{6}$$

Note that the backscatter cross section is defined as in units of area $[m^2]$. With $N_{tot} = 25800$ ppl we obtain a backscatter cross section representing an average for the ensemble of particles. The numerical value is $\sigma_{\pi,avg} = 2*10^{-11} m^2$. Obviously, this value is not very useful since the backscattered power can be assumed to depend on the particle size and this estimate applies really only for this particular size distribution. The size distribution can be incorporated only with some assumptions of the scattering properties of the objects. When the particle size is larger than the wavelength Rayleigh-MIE scattering relations [7] can

be used to approximate the backscattered power. Even if this case involves particles comparable to the wavelength we shall assume that the backscattering cross section is proportional to the mean projected area, $A_p = \pi d_p^2/4$, of the particle. We will find that this assumption can be of little significance for the end result. Using the definition of the backscattering efficiency, Q_π, related to the optical properties of the particles we can write

$$\sigma_\pi = Q_\pi A_p = \frac{Q_\pi \pi d_p^{\,2}}{4} \tag{7}$$

for the mean backscatter cross section from particles of one size. The volume backscatter function can now be expressed as

$$\beta = \frac{Q_\pi}{4\pi}[N_{0.5}A_{0.5} + N_1A_1 + N_2A_2 + N_3A_3 + N_5A_5 + N_{10}A_{10}]\,. \tag{8}$$

By assuming that the particle counter size parameter approximates the effective cross sectional diameter we obtain

$$\beta = \frac{Q_\pi}{16}[0,25N_{0.5} + N_1 + 4N_2 + 9N_3 + 25N_5 + 100N_{10}]*10^{-12}\,, \tag{9}$$

when the particles are grouped in size according to the particle counter output. It is evident that the larger particles give the greatest contribution to the backscattered radiation. Hence, under the assumption that the backscattering efficiency is independent of size or at least does not increase drastically for the smaller particles, we find that the contribution to the total backscatter from the smallest particles may be neglected unless the concentration by far exceeds that of the larger particles. Numerical values from the above discussed example give

$$\beta = Q_\pi[0.2 + 2 + 11 + 39 + 138 + 146]*10^{-7}\,, \tag{10}$$

where it is found that the smallest particles contribute insignificantly to the total backscattering. Using the above result $\beta \approx 3.9*10^{-5}$ $m^{-1}sr^{-1}$ derived from the measured heterodyne signal we obtain a revised estimate of the backscattering efficiency of the tested particles which is found to be

$$Q_\pi \approx 1.2 \ . \tag{11}$$

The uncertainty in this value is rather large due to many sources of errors e.g. the spread in the estimated heterodyne signal power, the particle counter uncertainty. We estimate that the real value is within a factor of four of this estimate. A thorough error analysis has not been made at this time. It should also be noted that the measured backscattering for this data was dominated by the two largest groups of particles which is making the uncertainty larger for the smaller particles. Other possible systematic errors are that;

-the particle concentration in the scattering volume differs from the measured concentration in the shower cabin

-the laser system parameters, in particular the visibility, depart from the calculated parameters.

-the measuring volume is underestimated

-the input coupling efficiency is overestimated (unity).

It should be emphasized that this estimated backscattering efficiency applies for the largest particles above about 3 μm since we have used data where the contribution to the backscattered power from the smaller particles was found negligible. Of course, a prerequisite for this assumption was that the backscattering efficiency is about the same for the smaller particles which has not been empirically established in any way in this work. A more accurate measurement would be required for that.

The following discussion may be of significance only if the number of scattering particles is relatively low with only one or a few particles contributing to the spectral power components. Judging from the particle counter data this was the case in our measurements due the small size of the measuring volume, 2.7 cm^3, from which the scattered light can be effectively collected. Since the measuring volume generally will increase rapidly with range, a larger number of scattering particles will contribute to the collected optical power at longer ranges.

Our attention is now focused on the two last series of data when the particle generator was turned off. It is evident, particularly from the last event (around 3550 minutes in figure 11) that the estimated backscattered power depends on the spectral resolution. A lower spectral resolu-

tion, in our case 100 kHz, seems to result in an underestimated backscattered power at low particle concentration levels. At the same time, it can be observed that the power drop resembles the drop of the particle concentration of the largest 10 micron sized particles, suggesting a rather simple explanation of the observed discrepancy.

When performing the integration in the frequency domain, the terms with power density below the threshold at $8*10^{-14}\ V^2/Hz$ are discarded. Since the power density is used, rather than the power in each frequency slot, signal components of lower peak power levels will contribute if the spectral resolution is increased. Our interpretation is that the backscattered power from the larger particles generate higher peak powers than that backscattered from smaller particles which is a natural (but not obvious) assumption as long as the number density of the scattering particles is relatively low. That is, if the signal generated in a frequency slot comes from light scattered by only one or a few particles, a larger particle may be required to generate sufficient heterodyne signal power. By using our result obtained for the backscattering efficiency Q_π of these particles the heterodyne signal power generated by a single particle can be estimated. We find that the backscattered power for a single particle can be written as

$$P_r = I\Omega Q_\pi A \tag{12}$$

with A denoting the projected area of the particle. The numerical values for the 2 and 10 micron particles become $P_r(2\mu)=1*10^{-13}\ W$ and $P_r(10\mu)=3*10^{-12}\ W$ respectively. The heterodyne signal power generated by the single particles is found by using equation (4), resulting in the numerical values $U^2(2\mu)=8*10^{-9}\ V^2$ and $U^2(10\mu)=2*10^{-7}\ V^2$. These values are to be compared to the detection threshold in the analysis which was set to $8*10^{-14}\ V^2/Hz$. Multiplication by the two chosen resolution bandwidths yields the two thresholds $U^2(12kHz)=9.6*10^{-10}\ V^2$ and $U^2(100kHz)=8*10^{-9}\ V^2$. This indicates that single particles with a size smaller than about 2 microns are undetectable at the 100 kHz resolution while single particles of larger size produce a detectable signal, above threshold, at both resolutions.

Equations (3), (4) and (8) tells us that a linear relationship is expected between the heterodyne signal power and the particle concentration. When the heterodyne signal power is compared to the particle count data in the final two series of data in figure 11 it is found that the rapid drop off above a level of approximately $1*10^{-7}\ V^2$ can be matched with fairly good agreement to the number density reduction of the 5 and the 10 micron particles. The total reduction in signal

power for the last series was found to be a factor of 50 (-17 dB) at 100 kHz resolution and a factor of 15 (-12 dB) at 12 kHz. At the same time, the particle counts dropped by a factor of 200, 20, 6, 5, 5, 1 for the size fractions 10, 5, 3, 2, 1, 0.5 microns respectively. Judging from this observation the smaller particles, from about 3 microns and down, contribute insignificantly to the signal power at 100 kHz but must be included to explain the power drop at the 12 kHz resolution. This result is not perfectly consistent with the single particle detection threshold calculated above which indicate that even 3 micron particles contribute to the signal power at 100 kHz resolution. Nonetheless, with respect to the uncertainty of the measurements a fairly good agreement can be claimed.

An important feature of the scattering particles is their velocity distribution. For signal power from two or more particles to add up at the same frequency the particles must have the same radial velocity. In our case, the frequency band in which the main signal power arises has a width of about 500 kHz leading to about 5 main frequency slots at 100 kHz resolution and about 42 frequency slots at 12 kHz resolution. Consequently it is less likely to see spectral components arising from multiple scattering particles at the 12 kHz resolution since the probability for this to happen is lower than at a lower resolution. At the same, the detection threshold in units of power is lower so that fewer particles are required in order to sum up to a detectable spectral power component. In fact, as long as the detected power is evenly distributed in a frequency band nothing is gained by increasing the spectral resolution, not until the resolution is high enough to distinguish between spectral components from single particles. In cases where this becomes possible, depending on parameters such as the measuring distance, the CLR receiving aperture and the CLR output power, it is possible to enhance the performance by increasing the resolution of the measurement. The crucial point is that the power from a single scattering particle will not generally disperse and consequently be more readily detected than several particles of smaller size summing up to the same power.

Having this said, it is necessary to discuss briefly the time domain properties of the particles. An assumption made about the scattering particle is that its velocity is constant during the period of time corresponding to the Fourier transform window. The window length in time units for our two cases is 20 μs and 160 μs. Since the average radial velocity of the particles is 0.5 m/s and the spread about 0.35 m/s, it is not likely that their velocity change much during time periods of the above scale. Moreover, as they reach only fractions of millimetres, we can

regard each measurement more or less as a frozen snapshot of the measuring volume. However, the final power spectrum is found by averaging periodograms along the full 5 ms waveform. During this time the particles move on the average 2.5 mm. Hence, some of the particles contributing to the power in each acquisition will be within the measuring volume only during a part of the total acquisition time in which case the averaging reduce their effective contribution to the signal power. A shorter period of averaging would circumvent this effect but to the cost of an increased detection threshold. Apparently, the performance will be critically dependent on both the spectral and the time domain settings in the analysis. It is likely that these parameters must be adapted to the physical properties of the scattering particles for optimum performance.

As was stated previously this discussion applies generally only for cases where the total number of particles is relatively low, at ranges where the backscattered power from single particles exceed the detection threshold of the system. In such cases the CLR can be operated in this enhanced mode [8] relying on discrimination of single particles.

An important consequence is that the detection limit in units of optical power will increase substantially at distances where enhance mode conditions no more prevail. As a matter a fact it is fair to say that this was the case in our situation as regards to detection of particles with a size smaller than approximately 2 microns.

A useful condition for detection is then that the signal power U_s divided by the effective signal bandwidth B_s must exceed the spectral density detection threshold S_{th}.

$$\frac{U_s^2}{B_s} > S_{th} \tag{13}$$

The relation can be used to estimate the number of particles required for detection. Using $B_s = 500\ kHz$ applying for our case we obtain the condition $U_s^2 > 4*10^{-8}$ V^2. The number of particles in the measuring volume is found by using the estimated power from each particle and assuming that it adds up incoherently. Approximately 5 particles with a size of about 2 μm are required while only a fifth of the power from a 10 μm particle is sufficient to overcome this limit. The corresponding particle densities at threshold are about 2000 ppl for 2 μm particles and 74 ppl for 10 μm particles at a range of 28 meter. The detection threshold is dependent of the signal bandwidth and a broader particle velocity distribution leads to an increased detection

threshold. If the particle concentration can be assumed to be constant within the scattering volume the threshold is independent of range. An increased scattering volume at longer ranges is compensated exactly by a reduction in the intensity and in the solid angle of detection provided the same optical system is used. However, since the measuring volume will increase rapidly with range, as R^4, this fact may be of limited use at longer ranges e.g. from a couple of 100 meters and up. To cope with longer ranges, the effective measuring volume can be reduced by using larger optics.

4. Conclusions and final remark

These tests have shown that bioaerosol particles are detectable using a CW CLR at a range of about 30 meters. A detectable signal was found down to particle concentration levels of approximately 4000 particles per litre (ppl) including all particles with a size parameter from 0.5 to 10 microns.

By using a heterodyne measurement technique the radial velocity distribution of the target cloud can be estimated without directional ambiguity.

Since the particle counter divided the particles in size groups it was possible to discern relationships between the backscattered power and particle size. The data was analysed under the assumption that the backscattered power is proportional to the cross sectional area of the particles, based on the MIE scattering theory. As the backscattered power for most of the data acquired under the above assumption can be traceable to the larger particles, from about 2 microns up to 10 microns, it is to this size range that we can apply our results.

The measurements at this range cannot be straightforwardly used to estimate the detection threshold at a longer range due to the short measuring distance, entailing conditions where single particle detection provided an enhanced mode of detection. However, by way of establishing the backscatter efficiency the performance at a longer range was estimated.

The backscatter efficiency of the particles was estimated to be $Q_\pi \approx 1$ with an estimated uncertainty of a factor of four. At long ranges the measuring volume, defined by the effective focal volume in a monostatic CLR system or by the intersection volume in a bistatic CLR, will be much larger and lots of particles will contribute to the detected backscattered power. The corresponding detection threshold for 2 micron particles, which can be considered to be a typi-

cal size in a practical application, was found to be approximately 2000 ppl. This threshold can be shown to be independent of range and aperture size in as much as the particles are uniformly distributed within the measuring volume. In practice, a longer range might require larger apertures to reduce the extent of the focal volume to adapt to the target cloud volume.

Actually, the only way to improve the performance for a CW CLR at long ranges is to increase the optical output power. An amplifier providing 10 Watts, commercially available today, would reduce the detection threshold by a factor of 25 (due to the quadratic relationship between the optical power and the heterodyne signal power). Thus, from 2000 ppl to 80 ppl for 2 micron particles. A much lower detection threshold than that is probably not going to be required to reach down to ambient particle concentration levels in most practical situations.

For short ranges like in this test we conclude that the detection threshold in terms of particle number concentration is critically dependent on particle size and that an enhanced mode operation is obtained when spectral components originating from scattering by single particles are distingishable. The enhance mode place certain requirements on the system. Firstly, the measuring volume must be small in order to keep the number of particles that contribute to the backscattered power low. Secondly, the optical power originating from a single particle must be high enough to overcome the system detection threshold. Under the assumption that the CW output intensity in the target area cannot be further increased it is possible either to enlarge the receiver aperture or to increase the spectral resolution in order to increase the signal to noise ratio (SNR). Such modifications could possibly extend the range to which single particle detection can provide an SNR enhancement.

A natural modification of the CLR system based on this work is to increase the output aperture in order to enable some degree of focusing at several hundred meters. As a consequence the bistatic arrangement may become impractical, if not impossible, to use. Hence, a monostatic arrangement will be implemented.

Note that this work remained unpublished until 2008, long after it was done (2002). We have now chosen to make an FOI report of it since the backscattering coefficient at 1.5 micrometer has now become a subject of interest within the frame of our work on BWA stand-off detection.

5. References

[1] F. Kullander, T. Carlsson, D. Letalick, M. Lindgren, “Particle cloud detection using coherent laser radar systems, step one”, FOI Swedish Defence Research Agency, Linköping, Technical report, FOI-R--0217--SE, November 2001.

[2] T. Carlsson and D. Letalick, “System setup and characterization, laser radar vibrometer at 1.55 μm,” FOI Swedish Defence Research Agency, Linköping, 2001, User report, FOI-D--0028--SE, November 2001.

[3] Bacillus Thuringensis (BT) is an insecticidal bacterium, marketed worldwide for control of many important plant pests - mainly caterpillars of the Lepidoptera (butterflies and moths) but also for control of mosquito larvae, and simulid blackflies that vector river blindness in Africa. Bt products represent about 1% of the total 'agrochemical' market (fungicides, herbicides and insecticides) across the world. The commercial Bt products are powders containing a mixture of dried spores and toxin crystals. They are applied to leaves or other environments where the insect larvae feed. The toxin genes have also been genetically engineered into several crop plants.

[4] Private communication with Tage Berglund at Swedish Defence Research Agency, Umeå.

[5] “Signal processing toolbox user’s guide, for use with Matlab”, Version 4, The Math Works Inc., 1998.

[6] B. E. A. Saleh and M. C. Tech, “Fundamental of photonics”, ISBN 0-471-83965-5, John Wiley & Sons Inc., 1991.

[7] F. G. Smith, “The infrared and electro-optical systems handbook-Atmospheric propagation of radiation”, Vol. 2, ISBN 0-8194-1072-1, IRIA and SPIE, 1996.

[8] R. L. McGann, “Flight test results from a low-power Doppler optical air data sensor”, Proc. SPIE Vol. 2464, pp. 116-124, 1995.